Role of the Binding Energy on Nondipole Effects in Single-Photon Ionization

M. Schmidt,[1] N. Melzer,[1] M. Kircher,[1] G. Kastirke,[1] A. Pier,[1] L. Kaiser,[1] P. Daum,[1] D. Tsitsonis,[1] M. Astaschov,[1] J. Rist,[1] N. Anders,[1] P. Roth,[1] K. Lin,[1] J. Drnec,[2] F. Trinter,[3] M. S. Schöffler,[1] L. Ph. H. Schmidt,[1] N. M. Novikovskiy,[4] Ph. V. Demekhin,[4] T. Jahnke,[5,6,*] and R. Dörner[1,†]

[1]*Institut für Kernphysik, Goethe-Universität Frankfurt, Max-von-Laue-Straße 1, 60438 Frankfurt am Main, Germany*
[2]*ESRF, The European Synchrotron, 71 Avenue des Martyrs, CS40220, 38043 Grenoble Cedex 9, France*
[3]*Molecular Physics, Fritz-Haber-Institut der Max-Planck-Gesellschaft, Faradayweg 4-6, 14195 Berlin, Germany*
[4]*Institut für Physik und CINSaT, Universität Kassel, Heinrich-Plett-Straße 40, 34132 Kassel, Germany*
[5]*Max-Planck-Institut für Kernphysik, Saupfercheckweg 1, 69117 Heidelberg, Germany*
[6]*European XFEL, Holzkoppel 4, 22869 Schenefeld, Germany*

(Received 22 December 2023; revised 15 March 2024; accepted 1 May 2024; published 4 June 2024)

We experimentally study the influence of the binding energy on nondipole effects in K-shell single-photon ionization of atoms at high photon energies. We find that for each ionization event, as expected by momentum conservation, the photon momentum is transferred almost fully to the recoiling ion. The momentum distribution of the electrons becomes asymmetrically deformed along the photon propagation direction with a mean value of $8/(5c)(E_\gamma - I_P)$ confirming an almost 100 year old prediction by Sommerfeld and Schur [Ann. Phys. (N.Y.) **396**, 409 (1930)]. The emission direction of the photoions results from competition between the forward-directed photon momentum and the backward-directed recoil imparted by the photoelectron. Which of the two counteracting effects prevails depends on the binding energy of the emitted electron. As an example, we show that at 20 keV photon energy, Ne^+ and Ar^+ photoions are pushed backward towards the radiation source, while Kr^+ photoions are emitted forward along the light propagation direction.

DOI: 10.1103/PhysRevLett.132.233002

What is the role of the photon's momentum in photoionization processes? Rich physics emerged in recent years from the search for answers to this fundamental question. Ionization processes for which this was discussed span from single-photon one- [1–11] and two-electron [12–14] processes of photoionization of atoms and molecules [15,16] in the perturbative regime to multiphoton and tunnel-ionization processes in strong laser fields [4,17–27]. Part of the answer is general and independent of the energy of the employed photons and their intensity: the energy transfer of E_γ from the light field to the atoms or molecules is accompanied by a momentum transfer of $k_\gamma = E_\gamma/c$, no matter if E_γ is the energy of a single photon or the sum energy of multiple photons, or even is a nonquantized amount of energy in very short strong light pulses. By momentum conservation, this momentum k_γ is, irrespective of the specifics of the process, given to the center of mass of the electron(s) and the ion in the final state of the ionization process. This holds not only for the usually discussed quantum mechanical expectation values of the momenta, but strictly on the level of individual ionization events. Because of the mass imbalance between photoelectron and photoion, however, the momentum is almost exclusively transferred to the ion in each ionization event. In the center-of-mass system, the electron and the ion are ejected with equal and opposite momentum. As this momentum corresponds to the kinetic energy of the photoelectron, it is usually orders of magnitude larger than k_γ showing a broad angular distribution (and, for some photoionization processes, also a broad distribution of its magnitude). Therefore, for quantum systems, a second question with respect to ensembles arises, which is conceptually different from the above question on the single-event level: what is the expectation value of the momentum of the electrons $\langle k_e^x \rangle$ and the ions $\langle k_i^x \rangle$ along the photon propagation direction (x)? It turns out, the answer to this question depends on the intensity of the light [4], the atomic species [8,9,28], for molecules on the molecular orientation [15], and, importantly, on the ionization potential I_p of the system. In the limit of adiabatic strong-field tunnel ionization without recollision, the prediction [4]

$$\langle k_e^x \rangle = \frac{E_\gamma - I_p}{c} + \frac{I_p}{3c} \tag{1}$$

has been confirmed experimentally [20]. The first term originates from the driving of the free electron in the electromagnetic field, while the momentum of $I_p/(3c)$ is transferred by the action of the magnetic field during the tunneling step [29]. For the case of single-photon ionization in the perturbative regime at high energies, i.e., in the

absence of any acceleration of the electron by the light field, the corresponding prediction is

$$\langle k_e^x \rangle = \frac{8}{5c}(E_\gamma - I_p). \tag{2}$$

In case of ionization, the photon energy has to be larger than the ionization potential. Accordingly, $\langle k_e^x \rangle$ is always forward directed. As mentioned above, the ion momentum is composed of two contributions: the forward-directed momentum of the photon and the backward-directed recoil by the photoelectron, leading to

$$\langle k_i^x \rangle = \frac{1}{5c}(-3E_\gamma + 8I_p). \tag{3}$$

This prediction dates back to Sommerfeld and Schur in 1930 [1]. The first terms in Eqs. (2) and (3) were confirmed experimentally only recently by Grundmann *et al.* [7] under conditions where the second terms were negligible. It is the purpose of this Letter to experimentally demonstrate the presence of the second terms (i.e., the role of the binding energy) and to rationalize the underlying physics. We will demonstrate that the role of I_p is crucial, as it determines whether ions are emitted in the forward or backward direction by the photoionization process, a question also relevant for determining the direction of radiation pressure in astrophysics [10,11].

To test this predicted influence of the binding energy, we have conducted a series of experiments at beamline ID31 of the European Synchrotron Radiation Facility (ESRF, Grenoble, France) in 16-bunch timing mode. We applied the COLTRIMS (cold target recoil ion momentum spectroscopy) technique [30–32] and crossed the synchrotron beam consisting of linearly polarized photons ($E_\gamma = 20$ keV, $k_\gamma = 5.36$ a.u.) with a supersonic gas jet of various rare-gas atoms with different I_p for K-shell ionization [Ne(1s) $I_p = 870$ eV, Ar(1s) $I_p = 3206$ eV, Kr(1s) $I_p = 14326$ eV]. Ions and electrons were guided by electric and magnetic fields towards two time- and position-sensitive detectors. From the times of flight and positions of impact, the initial momenta of ions and electrons after ionization were obtained. To improve the ion momentum resolution we used an electrostatic lens (see Fig. 2 in Ref. [33]) and a drift tube in the ion arm of the spectrometer. We achieved a 4π acceptance solid angle for ions with an energy of up to 1.5 eV and electrons of up to 2400 eV. In order to determine the mean value of the ion momenta, it is necessary to know the position of impact of ions with momentum zero on the detector. This zero is obtained from ions created by Compton scattering. For Compton scattering at high photon energies, the ion is a spectator to the binary momentum transfer between photon and electrons. Thus, the ions have almost zero momentum after the Compton process.

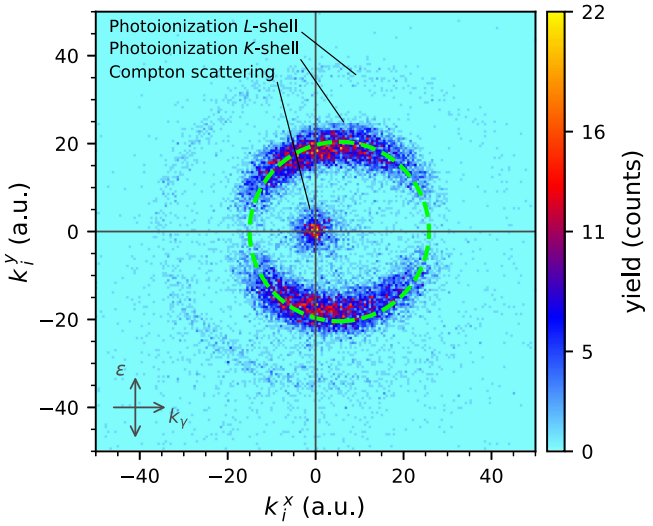

FIG. 1. Momentum distribution of Kr^{2+} ions from ionization by linearly polarized photons with $E_\gamma = 20$ keV. Horizontal axis: momentum component parallel to light propagation direction. Vertical axis: momentum parallel to polarization axis. The data shown are restricted to $|k_i^z| < 2.5$ a.u. The green dashed circle with a radius corresponding to the photoelectron momentum $k_e = \sqrt{2(E_\gamma - I_p)}$ is forward shifted by the photon momentum $k_\gamma = 5.36$ a.u.

Figure 1 shows the measured momentum distribution of Kr^{2+} ions recorded at a photon energy of 20 keV. For completeness, a full set of the measured distributions is reported in the Supplemental Material [34]. It shows a distinct peak at zero momentum resulting from ions created by Compton scattering. Two more circular features are visible in the experimental data. These originate from K-shell and L-shell photoionization, and correspond to the recoil imparted by the photoelectrons on the ions. The photoelectrons are emitted with a distinct kinetic energy and, accordingly, the ionization events are located on a sphere in momentum space with a radius corresponding to that energy, i.e., $k_e = \sqrt{2(E_\gamma - I_p)}$. In the representation chosen in Fig. 1, this sphere turns into a circular feature. The green dashed circle indicates the location of ions generated by K-shell ionization. Its radius is in accordance with the kinetic energy of K-shell photoelectrons and it is in addition forward shifted by the photon momentum ($k_\gamma = 5.36$ a.u.). Events belonging to L-shell ionization are located on a much larger circle (which is off centered, as well) and are faintly visible as indicated by the label, too. The Kr^{2+} photoions are in most cases a product of a two-step process of photoionization followed by Auger-Meitner decay. The additional recoil of the Auger electron leads to a broadening of the features in Fig. 1.

Figure 2 illustrates the central result of our study. For a given photon energy of $E_\gamma = 20$ keV, we plot the mean value of the ion and electron momenta along the light propagation direction, as functions of I_p. The blue line

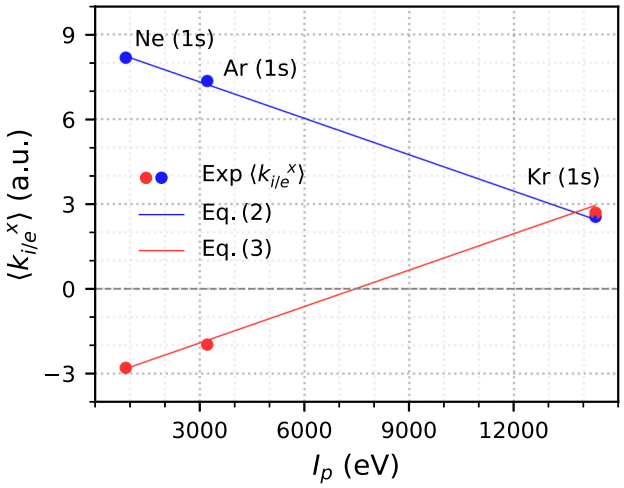

FIG. 2. Mean value of the measured electron (blue circles) and ion (red circles) momenta as functions of the binding energy I_p recorded at a photon energy of $E_\gamma = 20$ keV ($k_\gamma = 5.36$ a.u.). The statistical uncertainties are smaller than the size of the data points. Lines: predictions from Eqs. (2) and (3). Note that positive values of the mean momenta correspond to emission in the direction of the photon propagation.

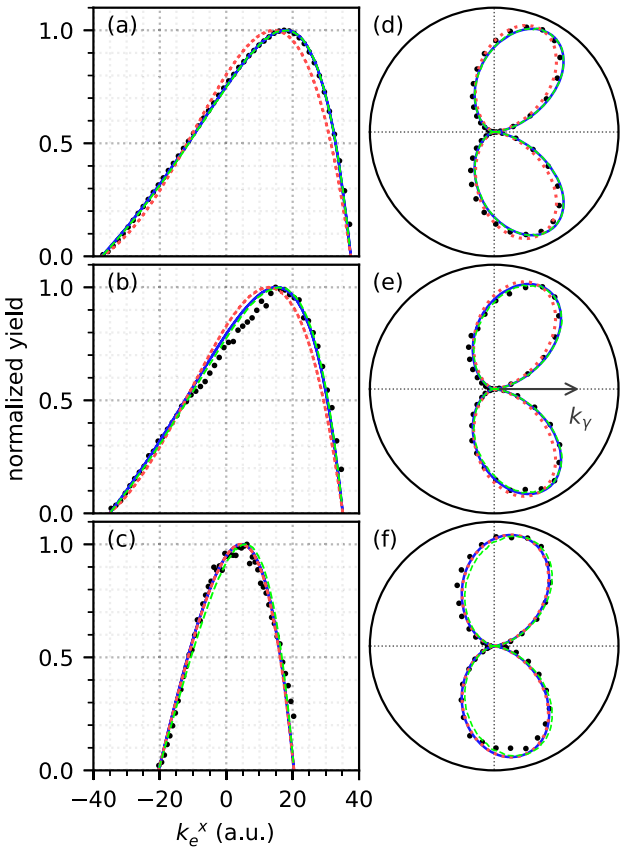

FIG. 3. Distributions of the photoelectron momentum k_e^x along the light propagation direction for (a) Ne, (b) Ar, (c) Kr, and photoelectron angular distributions for (d) Ne, (e) Ar, (f) Kr at a photon energy of $E_\gamma = 20$ keV ($k_\gamma = 5.36$ a.u.). The data are normalized to the maximum. Dots: experimental data, the statistical uncertainties are smaller than the size of the data points. Red dotted (blue solid) lines: theoretical calculations taking into account the first two expansion terms of the plane wave (the full $e^{i\mathbf{k}_\gamma \cdot \mathbf{r}}$) of the vector potential of the electromagnetic field. Green dashed lines: simulations via Eq. (4).

shows the prediction of Eq. (2), and the blue dots are the respective experimental results for K-shell photoelectrons of Ne, Ar, and Kr. The red line and dots show, respectively, the prediction of Eq. (3) and the measured results for the corresponding mean value of the ion momentum. The experimental data are in excellent agreement with the long-standing analytical predictions, including also the change of sign of the mean photoion momentum. Indeed, the Ne^+ and Ar^+ ions are emitted on average backwards, i.e., towards the light source, whereas Kr^+ ions are emitted in forward direction along the light propagation. Remarkably, for a binding energy of $I_p = (3/8)E_\gamma = 7.5$ keV [i.e., in between Fe(1s) $I_p = 7.1$ keV and Co(1s) $I_p = 7.7$ keV], photoions will stay on average at rest (for the given photon energy of $E_\gamma = 20$ keV).

To elucidate the underlying effect, we inspect the distributions of k_e^x, i.e., the differential cross sections $(\mathrm{d}\sigma/\mathrm{d}k_e^x)(k_e^x)$ in Fig. 3. As the photon momentum k_γ is transferred to the center of mass, i.e., rather to the ion than the electron, the photoion momenta are shifted in forward direction in good approximation by k_γ (see Fig. 1). As we will demonstrate below, the photoelectron momenta, in turn, are mostly affected by nondipole effects. In particular, these effects yield asymmetric electron momentum distributions along the light propagation direction, with a clear surplus of positive x momenta (see left panels of Fig. 3). The dipolar angular emission distributions (well known from low-energy photoionization) become clearly bent towards the light propagation direction (right panels of Fig. 3). With increasing binding energy, the photoelectron momentum distributions shown in Fig. 3 (left panels) get narrower, which reflects the lowering of the photoelectron energy $E_e = E_\gamma - I_p$. In addition, they become increasingly symmetric, which is also noticeable as a gradually smaller bending of the respective angular distributions occurs in the progression from Ne to Ar towards Kr atoms.

The physics behind the forward-backward asymmetry visible in Fig. 3 is most intuitively understood by considering photoionization in momentum space. In the perturbative regime of single-photon absorption, the photoelectron energy is independent of the intensity (i.e., the amplitude) of the electromagnetic wave. The electron is not accelerated, and, thus, the electron momentum is not altered by the driving field. Therefore, the electron momentum in the continuum [$k_e = \sqrt{2(E_\gamma - I_p)}$] needs to be present already in the initial (bound) state. Formally, this is captured in the Born approximation, where the final state of the electron is approximated by a plane wave in coordinate

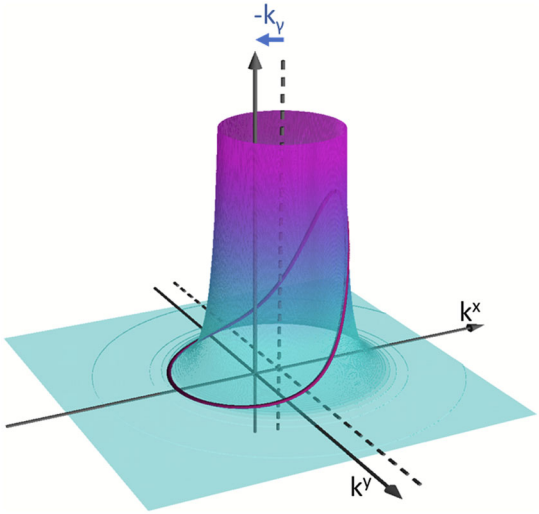

FIG. 4. Illustration of the role of the photon momentum in Eq. (4). The surface depicts a two-dimensional slice through the initial-state electron-momentum distribution, which is centered at the dashed coordinate frame. The red contour line shows the electron probability on a circle that is backward shifted by k_γ, highlighting the enhancement of the forward-directed electrons.

space. Photoionization samples the ground-state momentum distribution, selecting the part that allows us to match energy and momentum conservation. The ionization cross section is then proportional to the product of the probability to find the respective momentum in the ground state and the probability for inducing the transition from the bound to the continuum state. The latter is proportional to the square of the component of the electromagnetic field along the electron emission direction given by $\cos\theta_{\widehat{\mathbf{k}_e\epsilon}}$, where $\theta_{\widehat{\mathbf{k}_e\epsilon}}$ is the angle between the electron emission direction $\mathbf{k_e}$ and the polarization vector ϵ. This fact, that high-energy single-photon ionization directly samples the square of the Fourier transform of the bound state, is routinely exploited in angle-resolved photoemission spectroscopy (ARPES) in solid-state physics. For gas-phase molecules it has been successfully used to image correlated molecular orbitals [35].

The photon momentum factors into this approximation through evaluating the bound-state momentum distribution $\Psi_i(\mathbf{k}_e)$ on a sphere of radius k_e, which is centered not at momentum zero, but rather at $-\mathbf{k}_\gamma$, as illustrated in Fig. 4. Thus, the differential cross section can be estimated from this shifted-momentum distribution by evaluating the following integral:

$$\frac{\mathrm{d}\sigma}{\mathrm{d}k_e^x}(k_e^x) \propto \cos^2\theta_{\widehat{\mathbf{k}_e\epsilon}} \iint |\Psi_i(k_e^x - k_\gamma, k_e^y, k_e^z)|^2 \mathrm{d}k_e^y \mathrm{d}k_e^z \times \delta(E_e, E_\gamma - I_p), \tag{4}$$

with $E_e = \frac{1}{2}((k_e^x)^2 + (k_e^y)^2 + (k_e^z)^2)$. In this integral, we have used hydrogenlike initial wave functions in momentum space from Ref. [36] and the I_p for K-shell ionization of the respective atom. The results of the simulations via Eq. (4) are shown in Fig. 3 by the green dashed curves. They are in excellent agreement with the experimental results. The slight deviation of the experimental data from our simulations in Fig. 3(b) between −10 and +10 a.u. is most likely an artifact caused by spatial inhomogeneity of the detection efficiency of the microchannel-plate detector. In addition, we performed a systematic theoretical study of the photoelectron angular distributions, going beyond the hydrogenlike initial-state and the plane-wave final-state approximations. The calculations were performed within the Hartree-Fock approximation using the stationary single-center method [37–39], similarly to our previous studies on nondipole effects in molecules [6,15]. We used the velocity gauge for the photoionization transition matrix element and included partial electron continuum waves with angular momenta and projections up to ℓ, $|m| \leq 10$. In the calculations, the plane wave $e^{i\mathbf{k}_\gamma\cdot\mathbf{r}}$ of the vector potential, entering the transition matrix element, was treated either fully or by including only two terms in the respective expansion $e^{i\mathbf{k}_\gamma\cdot\mathbf{r}} \approx 1 + i\mathbf{k}_\gamma\cdot\mathbf{r}$. The results of the calculations are depicted in Fig. 3 by the blue solid and red dotted curves, respectively.

The Cartesian coordinate frame of Eq. (4) seems to account naturally for the linear momentum conservation and shift due to the photon momentum. This Cartesian coordinate perspective comes at the price that the description of the Coulomb potential and the initial state are less straightforward, and the angular momentum balance is not directly accessible. To account for these aspects, most theoretical approaches treat single-photon photoionization in spherical coordinates and expand the plane wave of the vector potential $e^{i\mathbf{k}_\gamma\cdot\mathbf{r}}$ in a Taylor series. Here, the first term approximating $e^{i\mathbf{k}_\gamma\cdot\mathbf{r}}$ by unity results in the dipole approximation, yielding forward-backward symmetric momentum distributions, while the asymmetries arise from higher (nondipole) expansion terms of the plane wave. A visualization of how an electric-quadrupole contribution bends the symmetric dipolar emission distribution of high-energy photoelectrons towards the light propagation direction can be found in our previous work [15] (see Fig. 1 and a respective discussion there). To further highlight this aspect, we display the electron emission distributions in spherical coordinates (right-hand panels of Fig. 3) and compare them to the results obtained from our modeling using different levels of approximation. We observe that for Ne, including electric-quadrupole and magnetic-dipole transitions (i.e., including the first two expansion terms $e^{i\mathbf{k}_\gamma\cdot\mathbf{r}} \approx 1 + i\mathbf{k}_\gamma\cdot\mathbf{r}$) is not fully sufficient at this photon energy, and higher nondipolar contributions need to be accounted to improve the agreement with the experiment. At the same photon energy for Ar, the nondipole contributions higher than electric quadrupole and magnetic dipole are much smaller, and for Kr almost irrelevant. This decreasing influence of nondipole contributions with

increasing binding energy originates from the fact, that the spatial region, which is relevant for the plane wave $e^{i\mathbf{k}_\gamma \cdot \mathbf{r}}$ in the transition amplitude, decreases with the square root of the binding energy. Thus, with increasing binding energy, the Taylor series converges more rapidly. Qualitatively, the distributions show a bending to the forward direction for all considered atoms. Importantly, this bending is not caused by the photon momentum directly, as this is absorbed by the ion. It is rather a consequence of the backward shift of the sphere in momentum space (see Fig. 4), on which the initial-state wave function is evaluated in Eq. (4).

In conclusion, we have provided stringent experimental support for the long-standing analytical prediction of how the photon momentum and the binding energy influence the momentum distributions of electrons and ions in single-photon ionization. Photoelectrons emerging from a K-shell are emitted forward with a mean momentum of $8/(5c)(E_\gamma - I_p)$. This momentum balance is determined by the electrons' ground-state momentum distribution and the photon momentum. The ion momentum $1/(5c)(8I_p - 3E_\gamma)$, in turn, results from the sum of two effects: the photon momentum, which is almost exclusively given to the heavy ion pushing it forward, and the recoil of the photoelectron, which at high energies is predominantly directed backwards. Which of the two effects prevails, i.e., whether the photoions are pushed forward or backward, depends on the binding energy. For the $1s$ orbital, the two effects cancel when the photon energy is equal $E_\gamma = (8/3)I_p$. Above that value, the photoions are emitted on average in the backward, and below in the forward direction.

We acknowledge the European Synchrotron Radiation Facility (ESRF) for provision of synchrotron radiation facilities under Proposal No. CH-6396 (DOI: 10.15151/ESRF-ES-878668690) and we would like to thank V. Honkimäki, H. Isern, and F. Russello for assistance and support in using beamline ID31. We acknowledge support by DFG. F. T. acknowledges funding by the Deutsche Forschungsgemeinschaft (DFG, German Research Foundation) - Project No. 509471550, Emmy Noether Programme.

*till.jahnke@xfel.eu
†doerner@atom.uni-frankfurt.de

[1] A. Sommerfeld and G. Schur, Ann. Phys. (N.Y.) **396**, 409 (1930).
[2] P. Auger and F. Perrin, J. Phys. Radium **8**, 93 (1927).
[3] O. Hemmers, R. Guillemin, and D. W. Lindle, Radiat. Phys. Chem. **70**, 123 (2004).
[4] S. Chelkowski, A. D. Bandrauk, and P. B. Corkum, Phys. Rev. Lett. **113**, 263005 (2014).
[5] M. Kircher, J. Rist, F. Trinter, S. Grundmann, M. Waitz, N. Melzer, I. Vela-Perez, T. Mletzko, A. Pier, N. Strenger, J. Siebert, R. Janssen, V. Honkimäki, J. Drnec, Ph. V. Demekhin, L. Ph. H. Schmidt, M. S. Schöffler, T. Jahnke, and R. Dörner, Phys. Rev. Lett. **123**, 193001 (2019).
[6] M. Kircher, J. Rist, F. Trinter, S. Grundmann, M. Waitz, N. Melzer, I. Vela-Pérez, T. Mletzko, A. Pier, N. Strenger, J. Siebert, R. Janssen, L. Ph. H. Schmidt, A. N. Artemyev, M. S. Schöffler, T. Jahnke, R. Dörner, and Ph. V. Demekhin, Phys. Rev. Lett. **123**, 243201 (2019).
[7] S. Grundmann, M. Kircher, I. Vela-Perez, G. Nalin, D. Trabert, N. Anders, N. Melzer, J. Rist, A. Pier, N. Strenger, J. Siebert, Ph. V. Demekhin, L. Ph. H. Schmidt, F. Trinter, M. S. Schöffler, T. Jahnke, and R. Dörner, Phys. Rev. Lett. **124**, 233201 (2020).
[8] O. Hemmers, G. Fisher, P. Glans, D. L. Hansen, H. Wang, S. B. Whitfield, R. Wehlitz, J. C. Levin, I. A. Sellin, R. C. C. Perera, E. W. B. Dias, H. S. Chakraborty, P. C. Deshmukh, S. T. Manson, and D. W. Lindle, J. Phys. B **30**, L727 (1997).
[9] R. Guillemin, O. Hemmers, D. W. Lindle, and S. T. Manson, Radiat. Phys. Chem. **73**, 311 (2005).
[10] G. Michaud, Astrophys. J. **160**, 641 (1970).
[11] M. J. Seaton, J. Phys. B **28**, 3185 (1995).
[12] M. Ya. Amusia, E. G. Drukarev, V. G. Gorshkov, and M. O. Kazachkov, J. Phys. B **8**, 1248 (1975).
[13] S. Grundmann, F. Trinter, A. W. Bray, S. Eckart, J. Rist, G. Kastirke, D. Metz, S. Klumpp, J. Viefhaus, L. Ph. H. Schmidt, J. B. Williams, R. Dörner, T. Jahnke, M. S. Schöffler, and A. S. Kheifets, Phys. Rev. Lett. **121**, 173003 (2018).
[14] H. Liang, S. Grundmann, Y.-K. Fang, L. Geng, Q. Gong, and L.-Y. Peng, Phys. Rev. A **104**, L021101 (2021).
[15] D. V. Rezvan, K. Klyssek, S. Grundmann, A. Pier, N. M. Novikovskiy, N. Strenger, D. Tsitsonis, M. Kircher, I. Vela-Peréz, K. Fehre, F. Trinter, M. S. Schöffler, T. Jahnke, R. Dörner, and Ph. V. Demekhin, Phys. Rev. Lett. **129**, 253201 (2022).
[16] S. Grundmann, D. Trabert. K. Fehre, N. Strenger, A. Pier, L. Kaiser, M. Kircher, M. Weller, S. Eckart, L. Ph. H. Schmidt, F. Trinter, T. Jahnke, M. S. Schöffler, and R. Dörner, Science **370**, 339 (2020).
[17] C. T. L. Smeenk, L. Arissian, B. Zhou, A. Mysyrowicz, D. M. Villeneuve, A. Staudte, and P. B. Corkum, Phys. Rev. Lett. **106**, 193002 (2011).
[18] S. Chelkowski, A. D. Bandrauk, and P. B. Corkum, Phys. Rev. A **95**, 053402 (2017).
[19] A. Ludwig, J. Maurer, B. W. Mayer, C. R. Phillips, L. Gallmann, and U. Keller, Phys. Rev. Lett. **113**, 243001 (2014).
[20] A. Hartung, S. Eckart, S. Brennecke, J. Rist, D. Trabert, K. Fehre, M. Richter, H. Sann, S. Zeller, K. Henrichs, G. Kastirke, J. Hoehl, A. Kalinin, M. S. Schöffler, T. Jahnke, L. Ph. H. Schmidt, M. Lein, M. Kunitski, and R. Dörner, Nat. Phys. **15**, 1222 (2019).
[21] S. V. B. Jensen, M. M. Lund, and L. B. Madsen, Phys. Rev. A **101**, 043408 (2020).
[22] S. Brennecke and M. Lein, Phys. Rev. A **98**, 063414 (2018).
[23] K. Lin, S. Eckart, A. Hartung, D. Trabert, K. Fehre, J. Rist, L. Ph. H. Schmidt, M. S. Schöffler, T. Jahnke, M. Kunitski, and R. Dörner, Sci. Adv. **8**, eabn7386 (2022).
[24] A. Hartung, S. Brennecke, K. Lin, D. Trabert, K. Fehre, J. Rist, M. S. Schöffler, T. Jahnke, L. Ph. H. Schmidt,

M. Kunitski, M. Lein, R. Dörner, and S. Eckart, Phys. Rev. Lett. **126**, 053202 (2021).
[25] Th. Keil and D. Bauer, J. Phys. B **50**, 194002 (2017).
[26] N. Haram, H. Xu, I. Ivanov, D. Chetty, I. Litvinyuk, and R. T. Sang, Phys. Rev. A **105**, 023522 (2022).
[27] K. Lin, S. Brennecke, H. Ni, X. Chen, A. Hartung, D. Trabert, K. Fehre, J. Rist, X.-M. Tong, J. Burgdörfer, L. Ph. H. Schmidt, M. S. Schöffler, T. Jahnke, M. Kunitski, F. He, M. Lein, S. Eckart, and R. Dörner, Phys. Rev. Lett. **128**, 023201 (2022).
[28] O. Hemmers, R. Guillemin, E. P. Kanter, B. Krässig, D. W. Lindle, S. H. Southworth, R. Wehlitz, J. Baker, A. Hudson, M. Lotrakul, D. Rolles, W. C. Stolte, I. C. Tran, A. Wolska, S. W. Yu, M. Ya. Amusia, K. T. Cheng, L. V. Chernysheva, W. R. Johnson, and S. T. Manson, Phys. Rev. Lett. **91**, 053002 (2003).
[29] M. Klaiber, E. Yakaboylu, H. Bauke, K. Z. Hatsagortsyan, and C. H. Keitel, Phys. Rev. Lett. **110**, 153004 (2013).
[30] R. Dörner, V. Mergel, O. Jagutzki, L. Spielberger, J. Ullrich, R. Moshammer, and H. Schmidt-Böcking, Phys. Rep. **330**, 95 (2000).
[31] J. Ullrich, R. Moshammer, A. Dorn, R. Dörner, L. Ph. H. Schmidt, and H. Schmidt-Böcking, Rep. Prog. Phys. **66**, 1463 (2003).
[32] T. Jahnke, Th. Weber, T. Osipov, A. L. Landers, O. Jagutzki, L. Ph. H. Schmidt, C. L. Cocke, M. H. Prior, H. Schmidt-Böcking, and R. Dörner, J. Electron Spectrosc. Relat. Phenom. **141**, 229 (2004).
[33] R. Dörner, V. Mergel, L. Spielberger, M. Achler, Kh. Khayyat, T. Vogt, H. Bräuning, O. Jagutzki, T. Weber, J. Ullrich, R. Moshammer, M. Unverzagt, W. Schmitt, H. Khemliche, M. H. Prior, C. L. Cocke, J. Feagin, R. E. Olson, and H. Schmidt-Böcking, Nucl. Instrum. Methods Phys. Res., Sect. B **124**, 225 (1997).
[34] See Supplemental Material at http://link.aps.org/supplemental/10.1103/PhysRevLett.132.233002 for momentum distributions of Kr^{2+}, Ar^{2+}, Ne^{2+}, and Ne^{+} ions.
[35] M. Waitz, R. Y. Bello, D. Metz, J. Lower, F. Trinter, C. Schober, M. Keiling, U. Lenz, M. Pitzer, K. Mertens, M. Martins, J. Viefhaus, S. Klumpp, T. Weber, L. Ph. H. Schmidt, J. B. Williams, M. S. Schöffler, V. V. Serov, A. S. Kheifets, L. Argenti, A. Palacios, F. Martín, T. Jahnke, and R. Dörner, Nat. Commun. **8**, 2266 (2017).
[36] R. Abrines and I. C. Percival, Proc. Phys. Soc. **88**, 861 (1966).
[37] Ph. V. Demekhin, A. Ehresmann, and V. L. Sukhorukov, J. Chem. Phys. **134**, 024113 (2011).
[38] Ph. V. Demekhin, D. V. Omel'yanenko, B. M. Lagutin, V. L. Sukhorukov, L. Werner, A. Ehresmann, K.-H. Schartner, and H. Schmoranzer, Opt. Spectrosc. **102**, 318 (2007).
[39] N. M. Novikovskiy, A. N. Artemyev, D. V. Rezvan, B. M. Lagutin, and Ph. V. Demekhin, J. Phys. B **55**, 175001 (2022).